INTERNATIONAL JOURNAL OF REMOTE SENSING, 2017
VOL. 38, NO. 2, 598–616
http://dx.doi.org/10.1080/01431161.2016.1268739

Taylor & Francis
Taylor & Francis Group

OPEN ACCESS

High spatial resolution burn severity mapping of the New Jersey Pine Barrens with WorldView-3 near-infrared and shortwave infrared imagery

Timothy A. Warner [a], Nicholas S. Skowronski [b] and Michael R. Gallagher [c]

[a]Department of Geology and Geography, West Virginia University, Morgantown, WV, USA; [b]USDA Forest Service, Northern Research Station, Morgantown, WV, USA; [c]USDA Forest Service, Northern Research Station, New Lisbon, NJ, USA

ABSTRACT

The WorldView-3 (WV-3) sensor, launched in 2014, is the first high-spatial resolution scanner to acquire imagery in the shortwave infrared (SWIR). A spectral ratio of the SWIR combined with the near-infrared (NIR) can potentially provide an effective differentiation of wildfire burn severity. Previous high spatial resolution sensors were limited to data from the visible and NIR for mapping burn severity, for example using the normalized difference vegetation index (NDVI). Drawing on a study site in the Pine Barrens of New Jersey, USA, we investigate optimal processing methods for analysing WV-3 data, with a focus on the pre-fire minus post-fire differenced normalized burn ratio (dNBR). Although the imagery, originally acquired with a 3.7 m instantaneous field of view, was aggregated to 7.5 m pixels by DigitalGlobe due to current licensing constraints, a slight additional smoothing of the data was nevertheless found to help reduce noise in the multi-temporal dNBR imagery. The highest coefficient of determination (R^2) of the regressions of dNBR with the field-based composite burn index was obtained with a dNBR ratio produced with the NIR1 and SWIR6 bands. Only a very small increase in R^2 was found when dNBR was calculated using the average of NIR1 and NIR2 for the NIR bands, and SWIR5 to SWIR8 for the SWIR bands. dNBR calculated using SWIR1 as the NIR band produced notably lower R^2 values than when either NIR1 or NIR2 were used. Differenced NDVI data was found to produce models with a much lower R^2 than dNBR, emphasizing the importance of the shortwave infrared region for monitoring fire severity. High spatial resolution dNBR data from WV-3 can potentially provide valuable information on finer details regarding burn severity patterns than can be obtained from Landsat 30 m data.

ARTICLE HISTORY
Received 24 August 2016
Accepted 20 November 2016

1. Introduction

The launch of DigitalGlobe's WorldView-3 (WV-3) sensor on 13 August 2014, opened new opportunities in satellite-borne mapping of wildland fire burn severity (Keeley 2009) using short wave infrared (SWIR; 1.4–2.5 μm) data at a finer spatial resolution than has been previously possible. A long history of research suggests that mapping of forest fire

CONTACT Timothy A. Warner Tim.Warner@mail.wvu.edu Department of Geology and Geography, West Virginia University, P O Box 6300, Morgantown, WV 26506-6300, USA

Table 1. WorldView-3 band centre wavelengths.

Band name	Band number	Centre wavelength (nm)	Spectral region[a]
Coastal Blue	1	426	Visible
Blue	2	481	Visible
Green	3	547	Visible
Yellow	4	605	Visible
Red	5	661	Visible
Red Edge	6	724	NIR
NIR1	7	832	NIR
NIR2	8	948	NIR
SWIR1	9	1210	NIR
SWIR2	10	1572	SWIR
SWIR3	11	1661	SWIR
SWIR4	12	1730	SWIR
SWIR5	13	2164	SWIR
SWIR6	14	2203	SWIR
SWIR7	15	2260	SWIR
SWIR8	16	2329	SWIR

See also Figure 1.
[a] For the purpose of this article, we define the visible as 0.4–0.7 μm, NIR 0.7–1.4 μm, and SWIR 1.4–2.5 μm.

burn severity is generally most effective with a spectral ratio that combines near-infrared (NIR; 0.7–1.4 μm) and SWIR (e.g. Garcia and Caselles 1991; Key and Benson 1999; Key 2006; Parks, Dillon, and Miller 2014). This ratio is especially successful if applied to imagery acquired immediately before and after the burn (Key and Benson 2006). The WV-3 sensor acquires eight visible (0.4–0.7 μm) and NIR bands, and unlike any previous high-spatial resolution sensor, can in addition acquire a further eight longer wavelength bands in the NIR and SWIR region (Table 1) (Kruse, Baugh, and Perry 2015; DigitalGlobe 2016). The eight visible and NIR WV-3 bands have a 1.2 m instantaneous field of view (IFOV), whereas the eight NIR and SWIR bands have an IFOV of 3.7 m, though currently this latter group of bands is degraded for the general public to 7.5 m pixels in accordance with licensing restrictions. Thus, WV-3 is significant both for its finer spatial resolution and its increased spectral resolution.

The importance of having access to high resolution SWIR data for mapping burn severity is demonstrated by Figure 1, which shows both the WV-3 bands and spectral reflectance

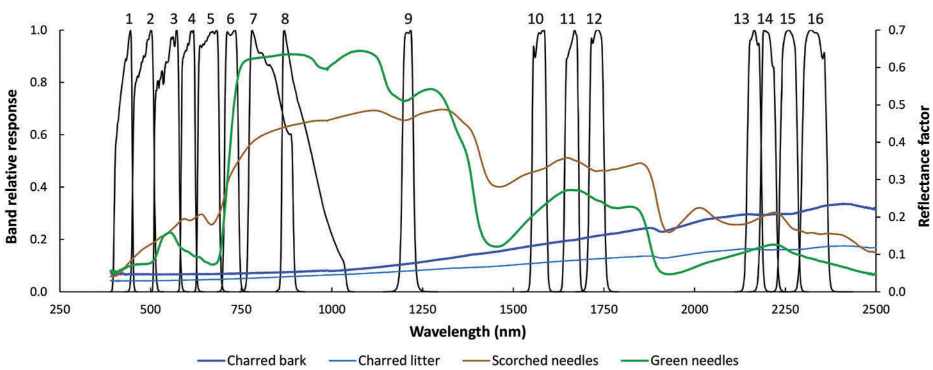

Figure 1. WorldView-3 band spectral response functions (left axis) by band (see numbers at the top of the graph) (DigitalGlobe 2016) and comparison to field spectral reflectance measurements of key cover types from the Penn State Forest.

field measurements of various land cover materials relevant for forest fire mapping. Compared to green pine needles, scorched pine needles show effects across the entire spectrum: increased blue and red, decreased NIR, and increased SWIR reflectance. Burnt plant matter, including litter and bark, which is black to the naked eye, has a generally low and featureless spectrum, although it does show a characteristic rise at longer wavelengths, resulting in characteristically SWIR reflectance that can be higher than that of green vegetation. The combination of reduced NIR and increased SWIR is, therefore, generally very effective for mapping burn severity (Key and Benson 1999, 2006).

Prior burn severity mapping has been mostly carried out using Landsat Thematic Mapper (TM), Enhanced Thematic Mapper Plus (ETM+), and Operational Line Imager (OLI) sensors, all with 30 m IFOV in the SWIR region (Garcia and Caselles 1991; Key and Benson 2006). Other satellite-borne sensors with SWIR bands that have been used for fire mapping include the Moderate Resolution Imaging Spectroradiometer (MODIS) with 500 m pixels (Chen, Sheng, and Liu 2015), the Advanced Spaceborne Thermal Emission and Reflection Radiometer (ASTER), with 30 m SWIR pixels (Holden et al. 2010), Satellite Pour l'Observation de la Terre (SPOT) 4 and 5 sensors with 20 m SWIR pixels (Polychronaki and Gitas 2012) and the European Space Agency's Multispectral Imager (MSI) on the Sentinel-2A satellite, also with 20 m pixels (Fernández-Manso, Fernández-Manso, and Quintano 2016). Thus, even with a degraded spatial resolution of 7.5 m, WV-3 data represents a substantial increase in potential detail over previously available satellite-borne sensors.

High spatial resolution mapping of burn severity from space-borne sensors could be particularly valuable for improved understanding of fire behaviour and for ecological restoration work, particularly for studying smaller fires in areas regarded as having high ecological value. For example, high resolution mapping could be useful for prescribed fires for forests close to inhabited areas, where the fires, though small, may be contentious and difficult to implement (Clark, Skowronski, and Gallagher 2015; Skowronski et al. 2015). Prior high spatial resolution sensors, such Airbus Defense & Space's Pléiades and DigitalGlobe's WorldView-2 (WV-2) sensors were limited to four, or at most eight, spectral bands, but crucially the bands were entirely within the visible to NIR range, typically no further than about 1.0 μm. Prior high spatial resolution sensors were therefore limited to mapping burn severity using visible and NIR wavelengths, for example using ratios such as the normalized difference vegetation index (NDVI; Rouse et al. 1974).

With its multiple high-spatial resolution SWIR bands, WV-3, therefore, offers significant opportunities for mapping burn severity. However, this new sensor also raises many questions that need to be addressed prior to routine use of the data. In particular, the choice of specific bands to use in developing the burn ratio is of some importance given that there are seven WV-3 SWIR bands and three NIR bands to select from. A related question is whether it is better to aggregate the SWIR bands, potentially to increase the signal to noise ratio, an approach that could be useful for winter acquisitions, when solar illumination is weak (Warner, Nellis, and Foody 2009). Furthermore, the eight visible and NIR bands are not necessarily provided as a package with the eight longer wavelength bands, raising another important issue as to whether effective burn severity mapping can be achieved using only the latter group of bands alone, especially since this group includes a NIR band at 1.2 μm. If a researcher only needs to purchase the eight longer wavelengths bands, this could result in considerable cost savings. In addition to addressing these methodological questions, we also ask whether, at least within the context of our study site, burn severity products generated at 7.5 m provide potentially more useful information than what can be discerned at 30 m, for example in a typical Landsat product. Finally, we also compare ratio products that use the SWIR band to NDVI, in order to confirm that the SWIR data really is useful for studying forest fire burn severity in our study area.

2. Background

The normalized burn ratio (NBR) is defined (Key and Benson 2006) as

$$\mathrm{NBR} = \frac{\rho_{\mathrm{NIR}} - \rho_{\mathrm{SWIR}}}{\rho_{\mathrm{NIR}} + \rho_{\mathrm{SWIR}}}, \tag{1}$$

where ρ is reflectance, and the subscripts NIR or SWIR describe the spectral regions. Generally, the 2.0–2.4 μm (e.g. Landsat TM band 7) atmospheric window is regarded as a better choice for the SWIR band than the 1.5–1.8 μm (e.g. TM band 5) window (Van Wagtendonk, Root, and Key 2004; Veraverbeke, Harris, and Hook 2011). There is a long history of the use of using a differenced NBR product (dNBR) to map burn severity (Key and Benson 2006; Escuin, Navarro, and Fernandez 2008):

$$\mathrm{dNBR} = (\mathrm{NBR})_{\mathrm{pre-fire}} - (\mathrm{NBR})_{\mathrm{post-fire}}, \tag{2}$$

where the subscripts pre-fire and post-fire refer to the timing of the acquisition of the imagery. In this article, we will apply the term dNBR to any differenced ratio images, employing NIR and SWIR bands, as defined earlier.

The dNBR measure has been found to be highly effective for mapping burn severity, particularly in forested environments (Van Wagtendonk, Root, And Key 2004; Key and Benson 2006). Nevertheless, variations on dNBR have been proposed to address shortcomings with the ratio. For example, a relative version of the dNBR can be used if there are large differences in the pre-fire canopy density (Miller and Thode 2007; Parks, Dillon, and Miller 2014). Another variation is to include spectral emissivity in the ratio (Fernández-Manso and Quintano 2015). For comparisons between multiple fires, an offset to the dNBR is sometimes applied to normalize the values so that they are comparable between fires (e.g. Miller et al. 2009). Entirely different approaches, such as machine-learning, have also been proposed where high spectral resolution data are available (Hultquist, Chen, and Zhao 2014).

Despite its success in forested environments, dNBR has been found to be less effective in other environments, such as grasslands (Lu, He, and Tong 2016). Similarly, Roy, Boschetti, and Trigg (2006) found that the ratio is not optimal for mapping fire in savannah vegetation.

Prior to the launch of WorldView-3, high spatial resolution sensors were generally limited to visible and NIR wavelengths. Typically, studies using such data have employed NDVI (Rouse et al. 1974) or similar vegetation indices. NDVI is defined as

$$\mathrm{NDVI} = \frac{\rho_{\mathrm{NIR}} - \rho_{\mathrm{Red}}}{\rho_{\mathrm{NIR}} + \rho_{\mathrm{Red}}}, \tag{3}$$

where, as before, ρ is reflectance, and the subscripts NIR or Red describe the spectral regions. A differenced NDVI index (dNDVI) can also be generated, as with dNBR, by differencing pre-fire and post-fire images. Many variations of NDVI and similar indices have been proposed to improve the effectiveness of using NIR and visible bands for mapping burn severity (Chuvieco, Martin, and Palacios 2002; Boelman, Rocha, and Shaver 2011).

Although NDVI is very reliable for measuring the presence of vegetation, the effect of burning can be confused with other losses of vegetation, and using NDVI to monitor burn severity is less effective if imagery is acquired when the vegetation has senesced. Many studies that have evaluated the use of high resolution dNDVI products have found them less effective than Landsat dNBR products (e.g. Escuin, Navarro, and Fernandez 2008). However, Holden et al. (2010) found that a differenced enhanced vegetation index (a modified version of NDVI) derived from QuickBird data produced a higher coefficient of determination (R^2) for regression models of field measures of burn severity than was achieved with Landsat TM dNBR data for a ponderosa pine study area in New Mexico, USA. Furthermore, Wu et al. (2015), in a study of ponderosa, pinyon, juniper, and oak forests in Arizona, USA, found that Landsat-derived dNDVI resulted in a higher R^2 than Landsat dNBR, or indeed than indices from WV-2 high-spatial resolution data, when regressed against burn severity.

In an important study using a radiative transfer model, Chuvieco et al. (2006) showed that a spectral ratio of NIR and red is potentially the most effective combination for mapping recent fires, where charcoal dominates the spectral signal. In contrast, ratios using NIR and SWIR provided the highest potential accuracy for a wider range of fires, both recent and older, and where soil, charcoal, and both green and brown leaves are present.

3. Study area

The study area is the Penn State Forest (Figure 2), in the New Jersey Pinelands National Reserve (PNR). Forests in this study area are primarily: ‘pine–oak forests’, consisting of pitch pine with mixed oaks in the overstory; ‘pine–scrub oak forests’, dominated by pitch pine with understory scrub oaks (*Q. ilicifolia* Wang. and *Q. marlandica* Muench.) in the understory (McCormick and Jones 1973; Lathrop and Kaplan 2004); or ‘pine plains’ which have a similar species assemblage to ‘pine-scrub oak forest’ but are characterized by very short statured stems (<2 m). Ericaceous shrubs are the major understory component of all of these forest types, primarily huckleberry (*Gaylussacia bacata* (Wang.) K. Koch, *G. frondosa* (L.) Torr. & A. Gray ex Torr.) and blueberry (*Vaccinium* spp.). The soils are sandy and acidic (La Puma, Lathrop, and Keuler 2013), and the topography is generally flat.

This landscape of the PNR is characterized by a high frequency and intensity of wildfires relative to other forest ecosystems in the northeastern USA. The study area has had a history of periodic wildfire events, with the largest occurring in 1948 and 1982 (La Puma, Lathrop, and Keuler 2013). These fires both burned a significant portion of Penn State Forest and there have been several smaller fires as well, most prior to 1982. Prescribed fire has been intermittently introduced to small, peripheral, stands within the study area with little effect on canopy fuel loading (H. Somes, New Jersey Forest Fire

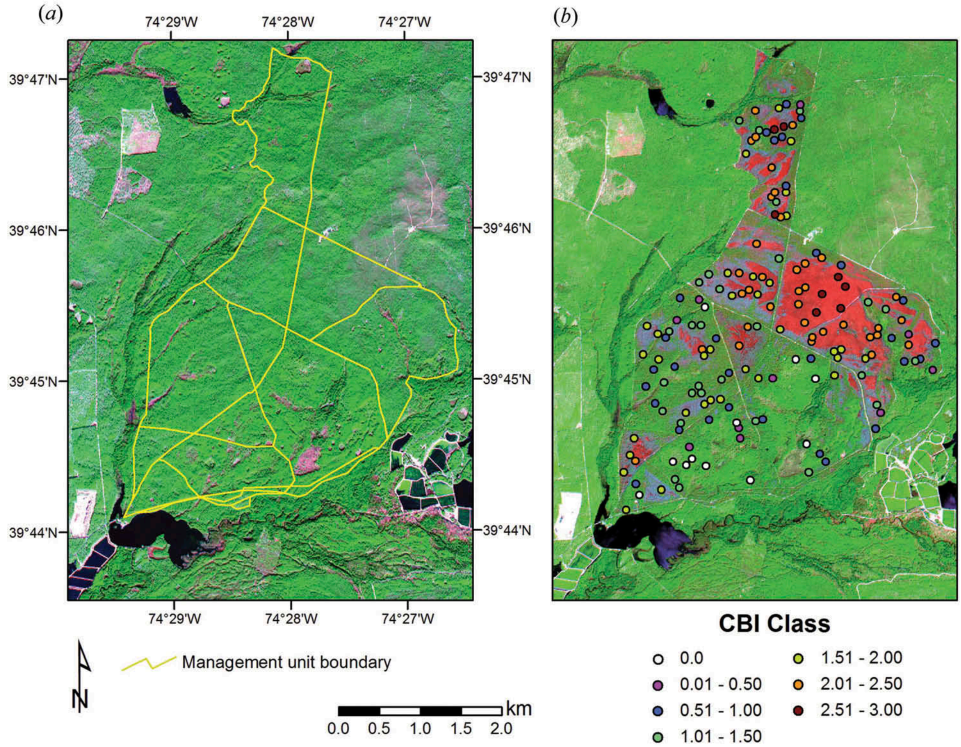

Figure 2. WorldView-3 false colour imagery (bands 16, 7, 5 as RGB) of Penn State Forest, New Jersey Pine Barrens. (*a*) Pre-burn image, acquired on 8 December 2015. (*b*) Post-burn image, acquired on 13 April 2016. Locations of field samples and associated Total CBI class are also indicated.

Service Division Fire Warden (*retired*), personal communication, 18 August 2016). For this study, nearly the entirety of Penn State Forest was burned on several days between 29 February and 18 March 2016. These burns were conducted under a wide range of meteorological conditions and fuel moistures with ignition patterns varying from backing, heading, and plastic sphere aerial ignition (many interior spot fires). An additional 150 ha within the study area burned in a wildfire on 10 March 2016.

4. Methods

4.1. *Field methods*

A total of 156 random samples were selected over the study site (Figure 2(*b*)). Although prior studies have selected samples using a stratified approach based on dNBR values (Key and Benson 2006) or site conditions (Kasischke et al. 2008), we chose a purely random approach combined with a relatively large number of samples to provide the simplest, direct, and most reliable estimate of the accuracy of the remotely sensed fire severity map. Our site is characterized by large areas of relatively low, moderate and intense burn intensities, making a purely random approach feasible. On the other hand, in an area without much variation in burn severity, a stratified approach might be necessary. Furthermore, we did not bias our selection to areas of relatively homogeneous burn severity, as is recommended by Key and Benson (2006). The disadvantage of our approach is that error in the georeferencing of the image or field sample locations will potentially translate into increased apparent spectral burn severity error, and result in an unnecessarily conservative estimate of overall accuracy. Nevertheless, we argue that it is highly possible that burn severity-estimation error is more common in mixed pixels, and therefore a sampling approach that systematically avoids areas of potential error would seem to be likely to generate an overly optimistic estimate of accuracy. For all these reasons, we argue that the approach we adopted produces the highest possible confidence in the accuracy estimates, and that, if anything, our approach is conservative.

The field measurements were made between 12 March and 6 April 2016, immediately after areas were burnt. Field procedures for estimating the composite burn index (CBI) employed the Key and Benson (2006) field data sheet. One key difference, however, is that we modified the diameter of the field plot from the recommended 30 m, to 15 m, in order to accommodate the finer scale of the WV-3 data compared to Landsat.

The CBI encompasses estimates of burn severity for five main strata of the vegetation: substrate, including litter and duff; herbs, low shrubs, and trees less than 1 m tall; tall shrubs and trees 1–5 m; intermediate trees, including sub-canopy and pole-sized trees; and big trees, including canopy, dominant and co-dominant trees (Key and Benson 2006). Within each stratum, burn-severity for each component within that stratum is estimated on a 0.0–3.0 scale. By averaging the burn severity values within each stratum, an index is obtained for that stratum. The values for the strata are then averaged to produce integrated understory, overstory, and overall burn indices.

Field spectra, shown in Figure 1, were collected on 12 March 2016, using a FieldSpec-2, portable field spectrometer (ASD Inc., Boulder CO, USA). A portable lamp provided by ASD was used for illumination, and spectra were normalized to a Labsphere (North Sutton, NH, USA) Spectralon barium sulphate reflectance standard (Asmaryan et al. 2013).

4.2. *Image acquisition, pre-processing and analysis*

A pre-fire image, including all 16 visible, NIR and SWIR bands, was acquired on 8 December 2015. (For convenience, we will refer to the bands by the numbers from 1–16, please refer to Table 1 for the associated wavelengths and the names given to the bands by DigitalGlobe.) As a winter scene, the sun elevation was 26.8°, and the mean off-nadir viewing angle was 6.3°. A post-fire image was acquired on 13 April 2016, with a notably higher sun elevation of 57.9° and a mean off-nadir viewing angle of 12.3°. The 4 month interval between the pre- and post-fire burn images is less than optimal in that any phenological changes in that time will likely reduce the accuracy of burn severity mapping. However, the acquisitions were timed to be after leaf senescence in the fall, and prior leaf expansion in the spring, and therefore plants were dormant in both images. In any case, given the challenges of acquiring snow-free and cloud-free images in the winter and early spring in the eastern United States, this period of time between acquisitions was the best we could achieve, and may be representative of what an operational fire monitoring programme would have to accommodate.

The images were imported in to ENVI 5.3 (Exelis Visual Information Solutions, Boulder, CO, USA). The images were converted into radiance, and then surface reflectance using the Fast Line-of-sight Atmospheric Analysis of Hypercubes (FLAASH) module within ENVI (Cooley et al. 2002). FLAASH is built around the MODTRAN radiative transfer model, and is able to deal with the non-nadir viewing effects.

The reflectance images were then imported into ERDAS Imagine 2015 (Hexagon Geospatial Inc., Norcross, GA, USA), and co-registered using the Imagine Autosync feature, which matches images using automatically generated tie-points. The images were then used to generate a variety of WV-3 dNBR ratio products, using bands 7, 8, or 9 as the NIR band, and one of the bands between 10 and 16 as the SWIR band (see Table 1 for the band designations, see Table 2 for the ratio combinations developed). In addition, two NDVI products (with band 6 for red and 7 or 8 as NIR) were generated. Broad-band NBIR ratio products were developed by averaging values across multiple NIR and SWIR bands, prior to calculating the ratios.

Table 2. Summary statistics for various dNBR products for describing composite burn index (CBI) values.

	Coefficient of determination (R^2)			
Spectral ratio[a]	CBI (total)	CBI (overstory only)	CBI (understory only)	Comment
(7 − 10)/(7 + 10)	0.810	0.852	0.474	
(7 − 11)/(7 + 11)	0.696	0.722	0.421	
(7 − 12)/(7 + 12)	0.828	0.844	0.521	
(7 − 13)/(7 + 13)	0.833	0.860	0.513	
(7 − 14)/(7 + 14)	**0.841**	0.866	0.522	
(7 − 15)/(7 + 15)	0.829	0.869	0.489	
(7 − 16)/(7 + 16)	0.839	**0.872**	0.507	
(8 − 10)/(8 + 10)	0.822	0.867	0.482	
(8 − 11)/(8 + 11)	0.683	0.807	0.455	
(8 − 12)/(8 + 12)	0.830	0.846	**0.527**	
(8 − 13)/(8 + 13)	0.828	0.856	0.510	
(8 − 14)/(8 + 14)	0.839	0.865	0.520	
(8 − 15)/(8 + 15)	0.828	0.870	0.488	
(8 − 16)/(8 + 16)	0.836	0.870	0.506	
(9 − 10)/(9 + 10)	0.728	0.737	0.469	
(9 − 11)/(9 + 11)	0.710	0.724	0.452	
(9 − 12)/(9 + 12)	0.727	0.700	0.524	
(9 − 13)/(9 + 13)	0.768	0.772	0.504	
(9 − 14)/(9 + 14)	0.774	0.778	0.509	
(9 − 15)/(9 + 15)	0.780	0.803	0.481	
(9 − 16)/(9 + 16)	0.795	0.811	0.502	
(7 − (10:12))/(7 + (10:12))	0.810	0.842	0.487	
(7 − (13:16))/(7 + (13:16))	***0.844***	***0.876***	***0.513***	
(7 − (13:15))/(7 + (13:15))	0.843	***0.876***	0.510	Similar to Landsat 8 dNBR
(8 − (10:12))/(8 + (10:12))	0.830	0.865	0.500	
(8 − (13:16))/(8 + (13:16))	0.841	0.875	0.511	
(9 − (10:12))/(7 + (10:12))	0.763	0.763	0.506	
(9 − (13:16))/(9 + (13:16))	0.795	0.807	0.509	
((7:8) − (10:12))/((7:8) + (10:12))	0.828	0.847	0.498	
((7:8) − (13:16))/((7:8) + (13:16))	***0.844***	0.865	***0.513***	
(7 − 5)/(7 + 5)	0.693	0.735	0.398	NDVI
(8 − 5)/(8 + 5)	0.647	0.680	0.381	NDVI

[a] See Table 1 and Figure 1 for key to band numbers.

The ':' symbol is used to indicate the average of a range of bands, e.g. '7:8' means bands the average of bands 7 and 8. Minimum and maximum R^2 values for single band ratios are shown, respectively, underlined and in bold. The maximum values R^2 for broad band ratios (using averages of multiple bands) are shown in bold italics.

Despite the Autosync co-registration, small differences between the December and April images could still be seen, when the images were overlaid. These appear to be real differences, reflecting differences in the shadowing and parallax effects from the different view angles and the varying tree heights. We, therefore, also developed a smoothed product, in addition to the raw dNBR images. The smoothed image was produced using a low-pass filter, where the values in a 3×3 pixel kernel follow a Gaussian curve, with a one-standard deviation (σ) of 0.85 (Brandtberg et al. 2003). We also used pixel aggregation to generate a dNBR product with a 30 m pixel size, to simulate the spatial resolution of Landsat imagery. We chose this approach of simulating a coarser resolution imagery, rather than using real Landsat data, in order to produce comparison images that only differed in spatial resolution.

For visualization of the images we followed a standardized procedure to develop a consistent mapping from dNBR to image colour. A linear stretch on a scale of 0–255 was applied to the dNBR values between a dNBR of 0 and the 99.95 percentile; values outside that range were saturated at 0 and 255, respectively. A standard ERDAS Imagine pseudo colour palette was then applied to the scaled values for all values above an empirically chosen threshold of 85; values below that value were shown in grey scale.

Two procedures were investigated for relating the dNBR values from the WV-3 imagery and the field samples. The key issues were that the centre of the field samples were not necessarily in the centre of a pixel and the field sampling was done over a 15 m diameter area, compared to the 7.5 m size of the pixels. The first method used the spectral values of the single pixel of Gaussian smoothed imagery, as discussed earlier, in which the point fell. The second approach used an area-weighted approach applied to the original, unsmoothed data. In this approach, a 15 m diameter circle was drawn around the centre of the field sample location. The proportion of the circle in each of the underlying pixels was then multiplied by the associated pixel reflectance, and the values summed. The two approaches produced almost identical results when the spectral values were regressed against CBI values. Although the low pass filter approach is much easier to implement, we chose the area weighted approach as being conceptually more appealing.

The various differenced WV-3 ratio data were regressed against the CBI data. Visual inspection indicated that the variables were non-linearly related, therefore, an exponential model was chosen.

5. Results and discussion

5.1. *Quantitative results*

Figure 3(*a*) summarises the average reflectance of the field sites, as measured in the 8 December 2015 WV-3 imagery, prior to the burn. The spectra are grouped based on the severity of burn, as estimated in the field, after the fire. The graph indicates the field sites were on average mostly similar, at least spectrally. However, the pixels that were classified as having the highest burn severity (i.e. CBI values of 2.5–3.0) had noticeably higher average SWIR reflectance prior to the burn, possibly indicating drier conditions in those areas (Van Leeeuwen 2009).

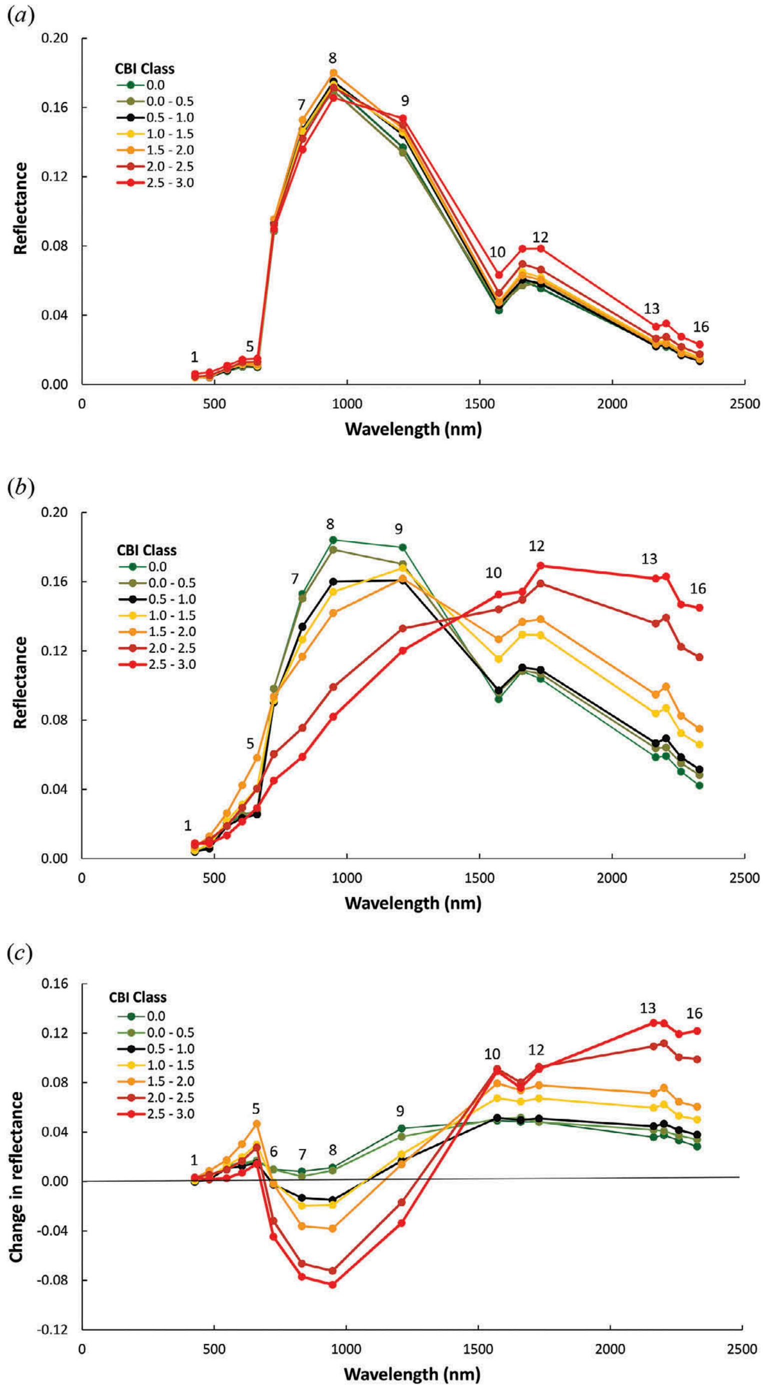

Figure 3. Average reflectance from WV-3 imagery for different classes of CBI. The numbers refer to the WV-3 band numbers (see Table 1). (*a*) Spectral reflectance from WV-3 imagery of 8 December 2016 (pre-fire). (*b*) Spectral reflectance from WV-3 imagery of 13 April 2016 (post-fire). (*c*) Change in spectral reflectance, from 8 December 2015 (pre-fire) to 13 April 2016 (positive values indicate reflectance increase).

Figure 3(*b*) shows the post-fire WV-3 reflectance spectra for the sample plots, also grouped by CBI value. Figure 3(*c*) shows the difference in reflectance between before and after the fire. Ideally, Figure 3(*c*) should show no change at all for the CBI class of 0.0, but in the SWIR bands in particular a reflectance change of approximately 0.04 is apparent. This could indicate real phenological changes in the 4 months between the two acquisitions as well noise, for example, due to uncertainties in the conversion to reflectance.

The results shown in Figure 3 are broadly consistent with the field spectra of Figure 1. In particular, the effect of fire is small and inconsistent in the visible, especially the red (band 5; 0.66 μm), where, with increasing CBI value, red reflectance first increases, most likely due to scorching of needles, but then decreases, as charred vegetation dominates. In contrast, in the NIR, particularly bands 7 (0.83 μm) and 8 (0.95 μm), there is a generally large and consistent decline in reflectance as CBI increases. For the NIR band 9 (1.2 μm) the change in reflectance is smaller than in the other NIR bands, and there is some inconsistency. For example, CBI class 0.5–1.0 is associated with a lower average reflectance than pixels with a CBI class of 1.0–1.5. The SWIR region also generally is associated with a large and consistent increase in reflectance as the CBI class increases, with the change greater in the longer 2.1–2.3 μm region (bands 13–16) than the shorter SWIR wavelengths of 1.6–1.7 μm (bands 10–12), particularly for the higher CBI value classes (i.e. more intensely burnt areas).

In summary, Figure 3 suggests that for the study area, NDVI is unlikely to be a useful measure of burn severity, particularly due to the relatively large and inconsistent change in red wavelengths. Furthermore, the NIR bands, 7 and 8 are likely to provide a more useful estimate of burn severity than 9. Of the SWIR bands (bands 10–16), the longer wavelength bands 13–16 appear to be the most useful.

Examples of the exponential regression models are shown in Figure 4; the complete results are listed in Table 2. Using CBI as the independent variable, and the differenced individual band dNBR data as the dependent variable, the exponential regression models resulted in coefficient of determination (R^2) values that vary from a low of 0.696 (using bands 7 and 11 as the NIR and SWIR bands, respectively) to a high of 0.841 (using bands 7 and 14). Notably, differencing using NDVI, the only option available in prior civilian high-resolution sensors, results in a much lower R^2 values of 0.647 and 0.693. These low R^2 values are consistent with the prediction of likely inconsistent NDVI changes with varying burn severity, as indicated by Figure 3.

Integrating adjacent NIR and/or adjacent SWIR bands was generally beneficial, so that overall the highest R^2 value of 0.844 was obtained where the NIR bands was band 7 alone or integrated with 8, and the SWIR bands was the average of bands 13–16. However, the difference in R^2 values between the single band and the broad band ratios is very small, only a matter of 0.004. The combination of bands designed to be similar to the spectral response of Landsat 8 OLI (band 7 for the NIR, and the average of bands 13–15 for the SWIR) results in a regression model with an R^2 very similar to the values for the data generated with the other broad-band differenced ratios.

The CBI is a summary measure based on both overstory and understory components. When the regression model is developed using the overstory component only, there is a small, but consistent increase in the R^2 values. The regression models built entirely on the CBI understory component have much greater scatter (Figures 4 (*e*) and (*f*)), and consequently a lower R^2, typically around 0.5 (Table 2). These results are not surprising; the understory is generally partially or totally obscured from the satellite view by the overstory. The overstory

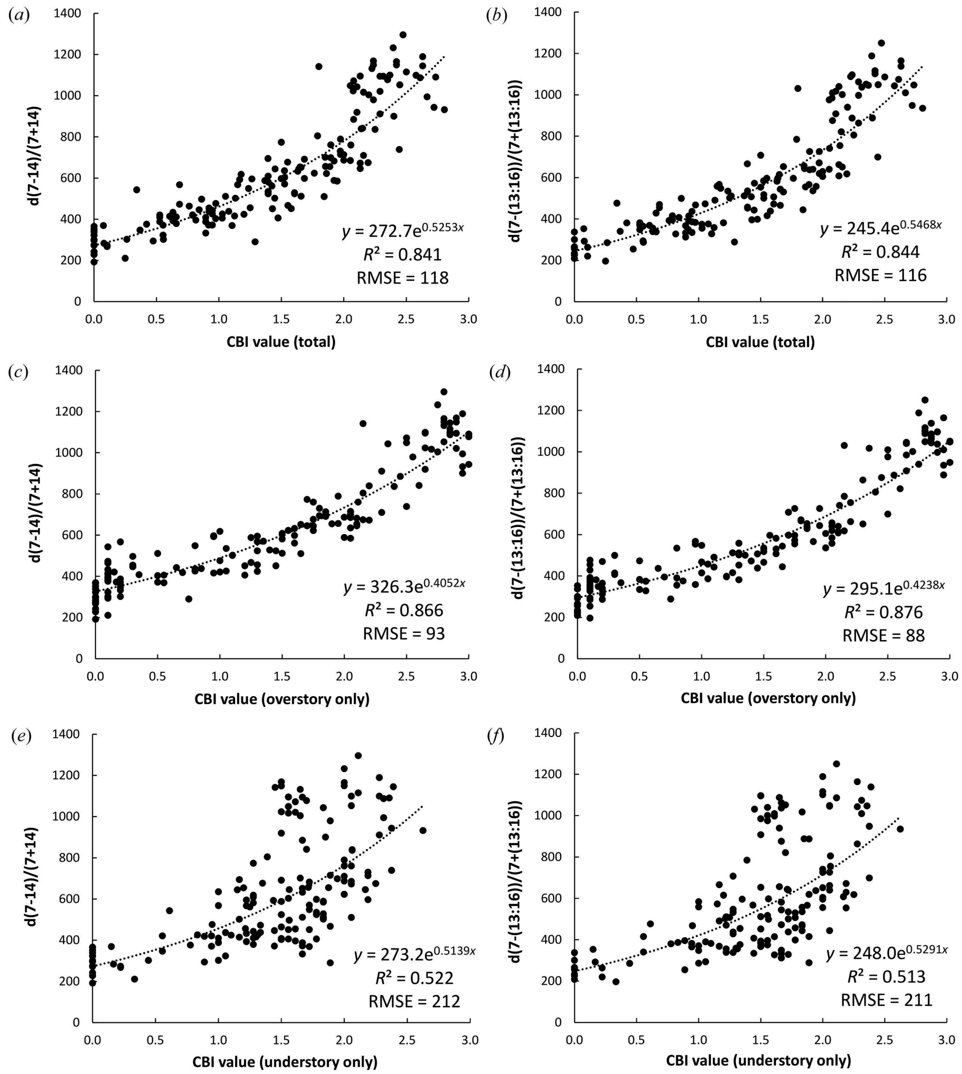

Figure 4. Scatterplots of CBI value versus example dNBR image ratios. Note that 'd' in the ratio is used to imply the before and after fires are differenced. (*a*), (*c*), and (*e*): Single band ratio using bands 7 and 14. (*b*), (*d*), and (*f*): Ratio using band 7 and integrated values from bands 12 to 14. (RMSE stands for root mean square error.)

clearly dominates in the satellite signal. One potential way of addressing this issue in future research would be to employ the GeoCBI of de Santis and Chuvieco (2009), which adjusts the estimate of CBI by fraction of cover of each layer. Such an approach might possibly result in an improved correlation between field and image estimates of burn severity.

5.2. *Visual analysis*

Figure 5(*a*) shows an example dNDVI image, and Figure 5(*b*) an example dNBR image. The dNDVI patterns are notably different from that of the nNBR image, and visually do

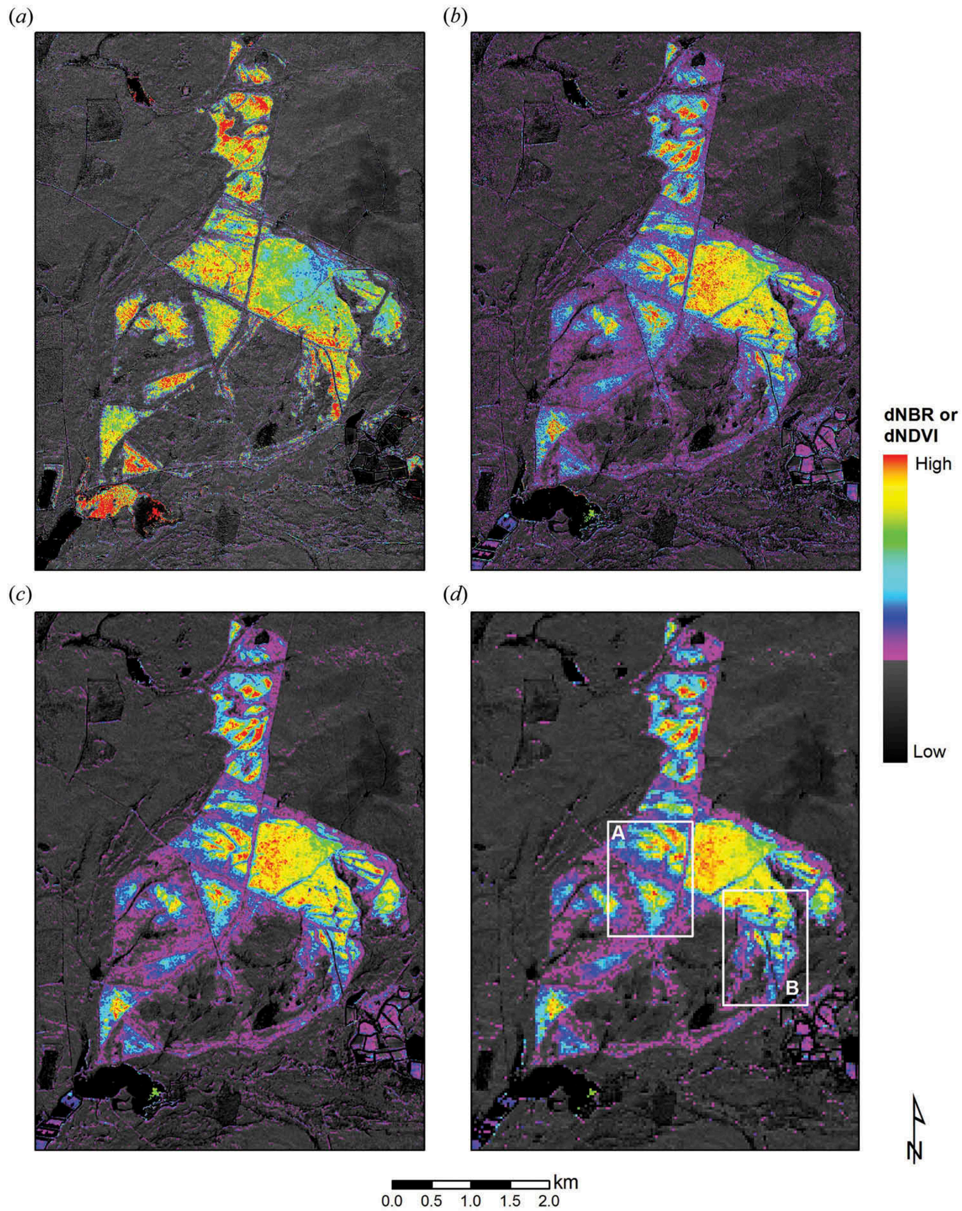

Figure 5. Differenced ratio images (pre-fire minus post-fire). (*a*) NDVI. (*b*) NBR using bands 7 and the average of bands 13–15 (i.e. d(7 – (13:15))/(7 + (13:15))). (*c*) The same as (*b*), only with a smoothing applied, to reduce noise. (*d*) The same as (*b*) only with 30 m pixels, to simulate the lower spatial resolution of Landsat 8 data. Rectangle A indicates the areas shown in detail in Figures 6 (*a*) and (*b*) and B indicates areas shown in Figures 6(*c*) and (*d*).

not appear to correspond well to the field burn severity measurements (Figure 2(*b*)). In particular, some of the largest dNDVI values, which are shown in red, have only small to moderate CBI changes. There is also a distracting change in NDVI in the lake in the southwest corner of the image (i.e. an area which was not burnt at all).

The differenced image at the original resolution (Figure 5(*b*)) has small, isolated areas of moderate values scattered throughout the unburnt area, which could be confused with a low severity burn. The Gaussian low pass filter suppresses much of this noise, whilst preserving the majority of the spatial patterns (Figure 5(*c*)). The fact that smoothing is apparently necessary, even though the WV-3 SWIR data are provided at 7.5 m

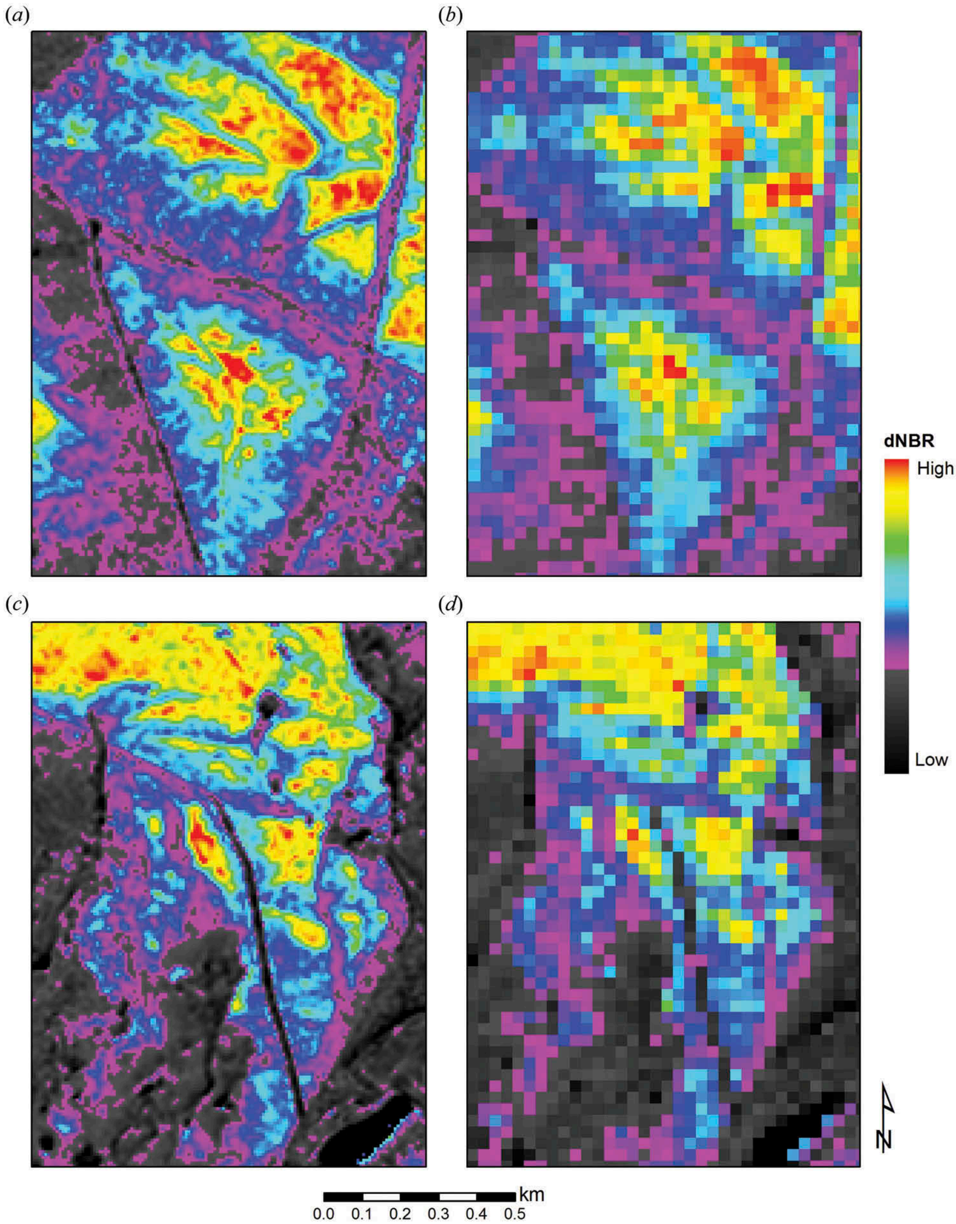

Figure 6. Detail of dNBR images. (*a*) and (*c*) show the ratio images with 7.5 m pixels. (*b*) and (*d*) illustrate the level of detail with 30 m pixels, equivalent to the spatial resolution of Landsat 8. (See Figure 5 for location information.)

resolution instead of the original 3.7 m IFOV, suggests that, at least for fire applications, the degradation of resolution to conform with the US licensing requirements may not matter greatly. Indeed, if at a future stage higher spatial resolution SWIR data is released, it is likely that users will need to apply an even greater smoothing prior to calculating the dNBR.

Other areas of moderate dNBR values that incorrectly indicate a low severity burn can be found in the southeast corner of Figure 5(*c*), where small, generally geometric regions of dominantly purple colour can be seen. Reference to Figure 2 indicates these areas are associated with changes in the water status in cranberry bogs, most likely due to drawing down of water levels in preparation for spring bud break.

Finally, we consider whether WV-3, with 7.5 m pixels, provides useful additional spatial information for monitoring wildland or prescribed fires. This is explored in the zoomed areas in Figure 5, shown in Figure 6. Figures 6(*a*) and (*c*) show the 7.5 m smoothed data, and Figures 6(*b*) and (*d*) the same areas, except with 30 m pixels. The 7.5 m data clearly shows the patterns in both high severity burns as well as the lower severity burn areas are much clearer. For example, in Figure 6(*a*), the fire spread patterns in the centre of the triangular field can be discerned with the 7.5 m pixels, but not 30 m pixels. Similarly, south of diagonal road, the 7.5 m data clearly shows two separate arms of high severity burn areas, which then coalesce. In the 30 m data, only a single high severity pixel is indicated. The 7.5 m data also shows notably more detail of burn patterns in low severity areas, sometimes in linear patterns possibly relating to differences in moisture or species composition, for example along drainage lines. This level of detail would be beneficial to studies focused on linking fine-scale environmental drivers of fire behaviour to the resulting severity.

6. Conclusions

The results of this study broadly indicate the value of WV-3 high spatial resolution (7.5 m) SWIR bands for monitoring burn severity. The high R^2 value (up to 0.844) for the regression of field-measured CBI values and the ratioed WV-3 data incorporating the SWIR bands provides strong empirical support that the fine detail of patterns observed in the imagery, such as in Figure 6, provides meaningful information about fine scale variations in burn severity. The NDVI-based mapping of burn severity was not a suitable alternative for this site.

The WV-3 SWIR data have an IFOV of 3.7 m, but were degraded to 7.5 m in terms of the DigitalGlobe licensing agreement. At some future date, the higher resolution data may be released. Our experience, in which a light smoothing using a Gaussian filter was important for reducing noise in the differenced ratio product, suggests that resolution finer than 7.5 m may open new challenges. At the very least, a more intense smoothing than that used in our work may be needed.

The eight bands acquired as part of the WV-3 SWIR package include-band 9 in the NIR, at 1.2 µm. It would, therefore, seem attractive to use this band as the NIR band in calculating the burn ratio instead of bands 7 or 8, from the VNIR bands, which potentially require a separate purchase. However, the best R^2 obtained with band 9 was 0.795, 0.049 lower than the 0.844 maximum obtained using band 7, or 7 and 8 combined. Thus, at least for this study site, there appears to be a distinct benefit in obtaining all 16 bands and not just the eight so-called SWIR bands.

Our recommendation is to use band 7 for the NIR band and 14 for the SWIR band, in the calculating dNBR. These two bands had the highest overall coefficient of determination using single bands, with an R^2 of 0.841. This was very close to the best R^2 when band 7, or 7 and 8 combined, were used as the NIR band and bands 13–16 combined as the SWIR band. In addition, the simulated broad-band Landsat OLI ratio resulted in a very similar R^2. Together, these results suggest that for burn severity mapping, the narrow bands of WV-3 produce potentially similar results to those of sensors with broader bands, such as Landsat 8 OLI or similar sensors. Thus, from the perspective of the user, it is probably simpler to use single bands, rather than to combine them. However, an important caveat is that, in our study, the topography was essentially flat. In rugged terrain, we recommend evaluating whether combining WV-3 bands 7 and 8 for the NIR band and 13–16 for the SWIR band improves the mapping of burn severity on poorly illuminated slopes (Veraverbeke et al. 2010).

WV-3 is a commercial satellite, and therefore purchasing the data require considerable financial outlay, unlike Landsat. This will of course constrain the use of data. Nevertheless, for fires of relatively small spatial extent, but of high value for ecological research or restoration or even perhaps for monitoring fires that encroach on structures in urban areas, the high resolution of the WV-3 data could be very valuable. High spatial resolution burn severity could be useful for relating to subsequent regrowth in leaf area index (Rachels et al. 2016), or for relating to other sensors, such as lidar (Skowronski et al. 2015), in order to study the linkages between fuel structure and loading to fire severity in ways that are not possible at a coarser resolution. This level of detail potentially provides important differentiation of fire spread patterns, and information that could be used for studying fire recovery.

An added benefit of WV-3 data is that the satellite is pointable, with a revisit time of potentially less than 1 day at 40° latitude, though this is reduced to 4.5 days if the off-nadir viewing angle is limited to less than 20°. This acquisition flexibility is valuable (Lippitt, Stow, and Riggan 2016), since in humid areas, such as the US East Coast, suitable pre- and post-fire Landsat data may not always be available due to clouds.

Acknowledgements

The authors would like to thank The New Jersey Forest Fire Service, particularly Section Warden Shawn Judy and the fire fighters of Section B2 for their help with this research. We are grateful to three anonymous referees, whose thoughtful comments greatly improved the article. We would also like to thank the USDA Forest Service for financial support through grant number 15-JV-11242306-084. Additional support was provided by grant number G14AP00002 from the Department of the Interior, United States Geological Survey to AmericaView and West Virginia View. The contents of this article are solely the responsibility of the authors and should not be interpreted as representing the opinions or policies of the US Government. Mention of trade names or commercial products does not constitute their endorsement by the US Government.

Disclosure statement

No potential conflict of interest was reported by the authors.

Funding

This work was supported by the USDA Forest Service [grant number 15-JV-11242306-084] and by the Department of the Interior, U.S. Geological Survey to AmericaView and West Virginia View [grant number G14AP00002].

ORCID

Timothy A. Warner http://orcid.org/0000-0002-0414-9748
Nicholas S. Skowronski http://orcid.org/0000-0002-5801-5614
Michael R. Gallagher http://orcid.org/0000-0003-0175-558X

References

Asmaryan, S., T. A. Warner, V. Muradyan, and G. Nersisyan. 2013. “Mapping Tree Stress Associated with Urban Pollution Using the Worldview-2 Red Edge Band.” *Remote Sensing Letters* 4 (2): 200–209. doi:10.1080/2150704X.2012.715771.

Boelman, N. T., A. V. Rocha, and G. R. Shaver. 2011. “Understanding Burn Severity Sensing in Arctic Tundra: Exploring Vegetation Indices, Suboptimal Assessment Timing and the Impact of Increasing Pixel Size.” *International Journal of Remote Sensing* 32 (22): 7033–7056. doi:10.1080/01431161.2011.611187.

Brandtberg, T., T. A. Warner, R. E. Landenberger, and J. B. McGraw. 2003. “Detection and Analysis of Individual Leaf-Off Tree Crowns in Small Footprint, High Sampling Density Lidar Data from the Eastern Deciduous Forest in North America.” *Remote Sensing of Environment* 85 (3): 290–303. doi:10.1016/S0034-4257(03)00008-7.

Chen, J., S. Sheng, and Z. Liu. 2015. “Detection of Annual Burned Forest Area Using Change Metrics Constructed from MODIS Data in Manitoba, Canada.” *International Journal of Remote Sensing* 36 (15): 3913–3931. doi:10.1080/01431161.2015.1055605.

Chuvieco, E., M. P. Martin, and A. Palacios. 2002. “Assessment of Different Spectral Indices in the Red-Near-Infrared Spectral Domain for Burned Land Discrimination.” *International Journal of Remote Sensing* 23 (23): 5103–5110. doi:10.1080/01431160210153129.

Chuvieco, E., D. Riaño, F. M. Danson, and P. Martin. 2006. Use of a Radiative Transfer Model to Simulate the Postfire Spectral Response to Burn Severity. *Journal of Geophysical Research: Biogeosciences* 111: G04S09. 10.1029/2005JG000143.

Clark, K. L., N. Skowronski, and M. Gallagher. 2015. “Fire Management and Carbon Sequestration in Pine Barren Forests.” *Journal of Sustainable Forestry* 34 (1–2): 125–146. doi:10.1080/10549811.2014.973607.

Cooley, T., G. P. Anderson, G. W. Felde, M. L. Hoke, A. J. Ratkowski, J. H. Chetwynd, J. A. Gardner, et al., 2002. “FLAASH, a MODTRAN4-Based Atmospheric Correction Algorithm, Its Application and Validation.” In *Geoscience and Remote Sensing Symposium, 2002. IGARSS’02. Vol. 3*, pp. 1414–1418. doi:10.1109/IGARSS.2002.1026134

de Santis, A., and E. Chuvieco. 2009. “GeoCBI: A Modified Version of the Composite Burn Index for the Initial Assessment of the Short-Term Burn Severity from Remotely Sensed Data.” *Remote Sensing of Environment* 113 (3): 554–562. doi:10.1016/j.rse.2008.10.011.

DigitalGlobe, 2016. “WorldView-3 Relative Radiometric Response Curves.” (Accessed June 212016). https://dg-cms-uploads-production.s3.amazonaws.com/uploads/document/file/208/WV03_technote_raduse_AttachmentA.pdf

Escuin, S., R. Navarro, and P. Fernandez. 2008. “Fire Severity Assessment by Using NBR (Normalized Burn Ratio) and NDVI (Normalized Difference Vegetation Index) Derived from LANDSAT TM/ETM Images.” *International Journal of Remote Sensing* 29 (4): 1053–1073. doi:10.1080/01431160701281072.

Fernández-Manso, A., O. Fernández-Manso, and C. Quintano. 2016. “SENTINEL-2A Red-Edge Spectral Indices Suitability for Discriminating Burn Severity.” *International Journal of Applied Earth Observation and Geoinformation* 50: 170–175. doi:10.1016/j.jag.2016.03.005.

Fernández-Manso, A., and C. Quintano. 2015. “Evaluating Landsat ETM+ Emissivity-Enhanced Spectral Indices for Burn Severity Discrimination in Mediterranean Forest Ecosystems.” *Remote Sensing Letters* 6 (4): 302–310. doi:10.1080/2150704X.2015.1029093.

Garcia, M. L., and V. Caselles. 1991. “Mapping Burns and Natural Reforestation Using Thematic Mapper Data.” *Geocarto International* 6 (1): 31–37. doi:10.1080/10106049109354290.

Holden, Z. A., P. Morgan, A. M. Smith, and L. Vierling. 2010. “Beyond Landsat: A Comparison of Four Satellite Sensors for Detecting Burn Severity in Ponderosa Pine Forests of the Gila Wilderness, NM, USA.” *International Journal of Wildland Fire* 19 (4): 449–458. doi:10.1071/WF07106.

Hultquist, C., G. Chen, and K. Zhao. 2014. “A Comparison of Gaussian Process Regression, Random Forests and Support Vector Regression for Burn Severity Assessment in Diseased Forests.” *Remote Sensing Letters* 5 (8): 723–732. doi:10.1080/2150704X.2014.963733.

Kasischke, E. S., M. R. Turetsky, R. D. Ottmar, N. H. French, E. E. Hoy, and E. S. Kane. 2008. “Evaluation of the Composite Burn Index for Assessing Fire Severity in Alaskan Black Spruce Forests.” *International Journal of Wildland Fire* 17 (4): 515–552. doi:10.1071/WF08002.

Keeley, J. E. 2009. “Fire Intensity, Fire Severity and Burn Severity: A Brief Review and Suggested Usage.” *International Journal of Wildland Fire* 18 (1): 116–126. doi:10.1071/WF07049.

Key, C. H. 2006. “Ecological and Sampling Constraints on Defining Landscape Fire Severity.” *Fire Ecology* 2 (2): 34–59. doi:10.4996/fireecology.0202034.

Key, C. H., and N. C. Benson 1999. “Measuring and Remote Sensing of Burn Severity.” In edited by L. F. Neuenschwander and K. C. Ryan, *Proceedings Joint Fire Science Conference and Workshop, Vol. II*, Boise, ID, June 15-17 1999. University of Idaho and International Association of Wildland Fire. 284 pp.

Key, C. H., and N. C. Benson 2006. “Landscape Assessment (LA). FIREMON: Fire Effects Monitoring and Inventory System.” *Gen. Tech. Rep. RMRS-GTR-164-CD*, Fort Collins, CO: US Department of Agriculture, Forest Service, Rocky Mountain Research Station. (Accessed 8 August 2016). Available from: http://www.fs.fed.us/rm/pubs/rmrs_gtr164/rmrs_gtr164_13_land_assess.pdf?

Kruse, F. A., W. M. Baugh, and S. L. Perry. 2015. “Validation of Digitalglobe WorldView-3 Earth Imaging Satellite Shortwave Infrared Bands for Mineral Mapping.” *Journal of Applied Remote Sensing* 9 (1): 096044. doi:10.1117/1.JRS.9.096044.

La Puma, I. P., R. G. Lathrop, and N. S. Keuler. 2013. “A Large-Scale Fire Suppression Edge-Effect on Forest Composition in the New Jersey Pinelands.” *Landscape Ecology* 28: 1815–1827. doi:10.1007/s10980-013-9924-7.

Lathrop, R., and M. B. Kaplan 2004. “New Jersey Land Use/Land Cover Update: 2000-2001”. *New Jersey Department of Environmental Protection*, 35 pp. (Accessed 19 August 2016). Available from: http://www.nj.gov/dep/dsr/landuse/landuse00-01.pdf

Lippitt, C. D., D. A. Stow, and P. J. Riggan. 2016. “Application of the Remote-Sensing Communication Model to a Time-Sensitive Wildfire Remote-Sensing System.” *International Journal of Remote Sensing* 37 (14): 3272–3292. doi:10.1080/01431161.2016.1196840.

Lu, B., Y. He, and A. Tong. 2016. “Evaluation of Spectral Indices for Estimating Burn Severity in Semiarid Grasslands.” *International Journal of Wildland Fire* 25 (2): 147–157. doi:10.1071/WF15098.

McCormick, J., and L. Jones 1973. “The Pine Barrens: Vegetation Geography.” *Research Report Vol. 3: New Jersey State Museum*. 76 pp.

Miller, J. D., H. D. Safford, M. Crimmins, and A. E. Thode. 2009. “Quantitative Evidence for Increasing Forest Fire Severity in the Sierra Nevada and Southern Cascade Mountains, California and Nevada, USA.” *Ecosystems* 12 (1): 16–32. doi:10.1007/s10021-008-9201-9.

Miller, J. D., and A. E. Thode. 2007. “Quantifying Burn Severity in a Heterogeneous Landscape with a Relative Version of the Delta Normalized Burn Ratio (dNBR).” *Remote Sensing of Environment* 109 (1): 66–80. doi:10.1016/j.rse.2006.12.006.

Parks, S. A., G. K. Dillon, and C. Miller. 2014. “A New Metric for Quantifying Burn Severity: The Relativized Burn Ratio.” *Remote Sensing* 6 (3): 1827–1844. doi:10.3390/rs6031827.

Polychronaki, A., and I. Z. Gitas. 2012. “Burned Area Mapping in Greece Using SPOT-4 HRVIR Images and Object-Based Image Analysis.” *Remote Sensing* 4 (2): 424–438. doi:10.3390/rs4020424.

Rachels, D. H., D. A. Stow, J. F. O’Leary, H. D. Johnson, and P. J. Riggan. 2016. “Chaparral Recovery following a Major Fire with Variable Burn Conditions.” *International Journal of Remote Sensing* 37 (16): 3836–3857. doi:10.1080/01431161.2016.1204029.

Rouse, J. Jr, R. H. Haas, J. A. Schell, and D. W. Deering 1974. “Monitoring Vegetation Systems in the Great Plains with ERTS.” *NASA Special Publication 351, Third Earth Resources Technology Satellite-1 Symposium. Volume 1*: 309–317. (Accessed 6 August 2016). Available from: http://ntrs.nasa.gov/search.jsp?R=19740022592

Roy, D. P., L. Boschetti, and S. N. Trigg. 2006. “Remote Sensing of Fire Severity: Assessing the Performance of the Normalized Burn Ratio.” *IEEE Geoscience and Remote Sensing Letters* 3 (1): 112–116. doi:10.1109/LGRS.2005.858485.

Skowronski, N. S., S. Haag, J. Trimble, K. L. Clark, M. R. Gallagher, and R. G. Lathrop. 2015. “Structure-Level Fuel Load Assessment in the Wildland-Urban Interface: A Fusion of Airborne Laser Scanning and Spectral Remote-Sensing Methodologies.” *International Journal of Wildland Fire* 25 (5): 547–557. doi:10.1071/WF14078.

Van Leeeuwen, W. J. D. 2009. “Chapter 3: Visible, Near-IR & Shortwave IR Spectral Characteristics of Terrestrial Surfaces.” In *The SAGE Handbook of Remote Sensing*, edited by T. A. Warner, M. D. Nellis, and G. M. Foody, 33–50. London, UK: SAGE.

Van Wagtendonk, J. W., R. R. Root, and C. H. Key. 2004. “Comparison of AVIRIS and Landsat ETM+ Detection Capabilities for Burn Severity.” *Remote Sensing of Environment* 92 (3): 397–408. doi:10.1016/j.rse.2003.12.015.

Veraverbeke, S., S. Harris, and S. Hook. 2011. “Evaluating Spectral Indices for Burned Area Discrimination Using MODIS/ASTER (MASTER) Airborne Simulator Data.” *Remote Sensing of Environment* 115 (10): 2702–2709. doi:10.1016/j.rse.2011.06.010.

Veraverbeke, S., W. W. Verstraeten, S. Lhermitte, and R. Goossens. 2010. “Illumination Effects on the Differenced Normalized Burn Ratio’s Optimality for Assessing Fire Severity.” *International Journal of Applied Earth Observation and Geoinformation* 12 (1): 60–70. doi:10.1016/j.jag.2009.10.004.

Warner, T., M. D. Nellis, and G. M. Foody. 2009. “Chapter 1: Remote Sensing Data Selection Issues.” In *The SAGE Handbook of Remote Sensing*, edited by T. A. Warner, M. D. Nellis, and G. M. Foody, 4–17. London, UK: SAGE.

Wu, Z., B. Middleton, R. Hetzler, J. Vogel, and D. Dye. 2015. “Vegetation Burn Severity Mapping Using Landsat-8 and Worldview-2.” *Photogrammetric Engineering & Remote Sensing* 81 (2): 143–154. doi:10.14358/PERS.81.2.143.